

# JGR Biogeosciences

## RESEARCH ARTICLE

10.1029/2021JG006764

### Key Points:

- The disequilibrium magnitude of global terrestrial carbon cycle showed dramatic reduction under the modeled nutrient limitation
- Nutrient limitation affects the disequilibrium magnitude primarily by dampening the productivity-driven changes
- Influences from changes in ecosystem carbon residence time are minor under the modeled nutrient limitation

### Supporting Information:

Supporting Information may be found in the online version of this article.

### Correspondence to:

J. Xia,  
jyxia@des.ecnu.edu.cn

### Citation:

Wei, N., Xia, J., Wang, Y.-P., Zhang, X., Zhou, J., Bian, C., & Luo, Y. (2022). Nutrient limitations lead to a reduced magnitude of disequilibrium in the global terrestrial carbon cycle. *Journal of Geophysical Research: Biogeosciences*, 127, e2021JG006764. <https://doi.org/10.1029/2021JG006764>

Received 19 DEC 2021

Accepted 13 APR 2022

## Nutrient Limitations Lead to a Reduced Magnitude of Disequilibrium in the Global Terrestrial Carbon Cycle

Ning Wei<sup>1,2,3</sup>, Jianyang Xia<sup>1,2</sup> , Ying-Ping Wang<sup>4</sup> , Xuanze Zhang<sup>1,2</sup>, Jian Zhou<sup>1,2</sup>, Chenyu Bian<sup>1,2</sup>, and Yiqi Luo<sup>3</sup> 

<sup>1</sup>Research Center for Global Change and Complex Ecosystems, School of Ecological and Environmental Sciences, East China Normal University, Shanghai, China, <sup>2</sup>State Key Laboratory of Estuarine and Coastal Research, Research Center for Global Change and Ecological Forecasting, East China Normal University, Shanghai, China, <sup>3</sup>Center for Ecosystem Science and Society, Northern Arizona University, Flagstaff, AZ, USA, <sup>4</sup>CSIRO Oceans and Atmosphere, Aspendale, VIC, Australia

**Abstract** The terrestrial carbon (C) cycle is shifting to a state of dynamic disequilibrium under a rapid global climate change. However, the magnitude of such disequilibrium is inherently hard to measure directly. Abundant studies have revealed that the availability of nutrients, particularly nitrogen (N) and phosphorus (P), constrains ecosystem productivity and carbon stocks across the globe. However, whether and how nutrient limitation affects the disequilibrium magnitude of the terrestrial C cycle ( $X_p$ ) has never been evaluated. Here, we developed an approach by combining a process-based numerical model and an analytical framework to evaluate the role of nutrient limitation on  $X_p$ . We found that nutrient limitation did have significant impacts on the  $X_p$ . Over the modeled period of 1901–2013, absolute change in  $X_p$  was 497.6 PgC under the C-only run, while it decreased to 155.6 and 124.3 PgC under N and NP limitations, respectively. To understand the underlying reasons, we further disaggregated the changes of  $X_p$  into changes in steady-state C storage and transit C storage with the former being decomposed into a productivity-driven change, an ecosystem-C-residence-time-driven ( $\tau_E$ -driven) change, and a change induced by productivity- $\tau_E$  interactions. We found that nutrient constrained the increase in  $X_p$  primarily by dampening the productivity-driven changes in the steady-state C storage. Reductions in the productivity-driven term under N and NP limitations accounted for 94.7% and 94.9%, respectively, of the reductions in the steady-state C storage. These results indicate that nutrient limitations have profound impacts on future climate-biosphere feedback by reducing the disequilibrium magnitude of the terrestrial C cycle.

**Plain Language Summary** The steady-state assumption is prevalent in terrestrial carbon (C) cycle studies, where C influxes are assumed to balance against C effluxes. However, climate change and other disturbances have caused dynamic disequilibrium of the terrestrial C cycle. The disequilibrium magnitudes of the terrestrial C sink and source vary over time under disturbances. Nutrient limitation, particularly from N and P, is widely acknowledged as one of the influential factors to the terrestrial C sink. It remains unknown whether and how nutrient limitation affects the disequilibrium magnitude of the terrestrial C cycle ( $X_p$ ). In this study, we first used an analytical way to estimate the  $X_p$  and further proposed a framework to disaggregate controls on the dynamics of  $X_p$ . We then applied the analytical framework to a C-N-P-coupled land-surface model to investigate the role of nutrient limitation on the  $X_p$ . We found a significant nutrient limitation on the  $X_p$ . Over the modeled period, the absolute change in  $X_p$  was reduced by 68.7% and 75.0% under N and NP limitations, respectively. These results indicate that nutrient availability can regulate the pattern of dynamic disequilibrium in the terrestrial C cycle under future climate change.

## 1. Introduction

Anthropogenic carbon (C) emissions from fossil fuel combustion and land-use change have resulted in a rapid increase in atmospheric CO<sub>2</sub> concentration and climate change (Canadell et al., 2007; Le Quéré et al., 2018; Zaehle, 2013). These unprecedented changes in the climate system have caused the dynamic disequilibrium (or instability) of the terrestrial C cycle (Luo & Weng, 2011), that is, the sink and source behaviors of the terrestrial C cycle and the disequilibrium magnitude vary over time in response to a global change. For example, rises in atmospheric CO<sub>2</sub> concentration have stirred the preindustrial C cycle, which stimulates plant C uptake, thus enhancing the strength of terrestrial C sink. Over the last half-century, the terrestrial C sink nearly tripled in magnitude, increasing from  $1.3 \pm 0.4$  GtC yr<sup>-1</sup> in the 1960s to  $3.4 \pm 0.9$  GtC yr<sup>-1</sup> in the 2010s (Friedlingstein

et al., 2020). However, the CO<sub>2</sub> fertilization effect on terrestrial C sequestration is not infinite due to nutrient limitation, particularly nitrogen (N) and phosphorus (P) limitations (Hessen et al., 2004; Vitousek et al., 2010). Based on the concept of dynamic disequilibrium (Keenan & Williams, 2018; Luo et al., 2017; Luo & Weng., 2011; Odum, 1969), disturbances and climate change lead to disequilibrium of the C cycle, while internal C processes (i.e., C assimilation, partitioning, and decomposition) drive the ecosystem recovering toward a steady state. It is thus reasonable to assume that nutrient limitation on C sequestration in a CO<sub>2</sub>-enriched environment might result from nutrient influences on both the internal C processes and the disequilibrium magnitude of the terrestrial C cycle.

Nutrient limitations on terrestrial C processes, especially vegetation productivity, have been widely observed at both the site level (Elser et al., 2007; Menge & Field, 2007; Oren et al., 2001; Reich et al., 2006; Sionit et al., 1981) and the global scale (e.g., Elser et al., 2007; Oren et al., 2001; Sionit et al., 1981; van Groenigen et al., 2006; Xia & Wan, 2008). Not only the productivity but also the C allocation can be affected by the availability of nutrients. Under nutrient limitations, for example, plant tends to allocate more sequestered C to below-ground for fine root production and root exudation rather than stored in long-lived C compartments (Hofhansl et al., 2016). Additionally, the nutrient limitation could affect both the quantity and the quality of produced litter, altering the decomposition processes (Averill & Waring, 2017) and soil C storage (Crowther et al., 2019). However, how nutrient limitation would influence the disequilibrium magnitude of the terrestrial C cycle is unknown as it is hard to estimate in field studies. Terrestrial ecosystems act as C sinks or sources only when the C cycle is at disequilibrium (Keenan & Williams., 2018; Luo & Weng., 2011). The dynamic of disequilibrium magnitude can be a good indicator of the behavior of the terrestrial C cycle (Luo & Weng., 2011). Therefore, understanding how nutrient limitation changes the disequilibrium magnitude of the terrestrial C cycle could have important implications for predicting future land C sink strength.

The disequilibrium magnitude of the terrestrial C cycle can be estimated as the difference between ecosystem C stocks at the steady and transit states (Luo et al., 2017). The concept of disequilibrium magnitude has two inferences: (a) when the transient C stock is smaller (larger) than the steady-state C storage, the disequilibrium magnitude is positive (negative) and the ecosystem could be potential C sink (source); (b) the uneven responses of transient and steady-state C stocks to disturbances and climate change will lead to the disequilibrium magnitude varying over time. Thus, impacts of nutrient limitation on the disequilibrium magnitude of the terrestrial C cycle depend on how nutrient availability regulates those key C processes that influence transient and steady-state ecosystem C stocks differently. Specifically, the dynamic of transient ecosystem C stock is determined by the balance between photosynthetic C input (i.e., net primary productivity; NPP) and multiple pathways of C losses (Keenan & Williams, 2018). The steady-state ecosystem C stock is determined by net primary productivity (NPP) and ecosystem C residence time ( $\tau_E$ ), which measures how long the inputted C can reside in an ecosystem (Sierra et al., 2017; Xia et al., 2013). Thus, the critical step to studying nutrient limitation on the disequilibrium magnitude is to know how the abovementioned processes change under different nutrient conditions. Changes in C influxes and effluxes are measurable in the natural ecosystem. However, changes in  $\tau_E$  are determined by a myriad of biological processes, and some of these processes cannot be directly measured (Lu et al., 2018). Thus, the dynamics of  $\tau_E$  are usually studied by modeling simulations and theoretical analyses (Lu et al., 2018; Sierra et al., 2017).

Global land-surface models are widely used for understanding the long-term and large-scale terrestrial C cycle (Fisher et al., 2014; Fisher & Koven, 2020; Huntzinger et al., 2013). The tight interactions involving C, N, and P cycles have long been acknowledged as one of the most important factors determining the future terrestrial C-cycle-climate feedbacks (Elser et al., 2007; Oren et al., 2001; Sionit et al., 1981; van Groenigen et al., 2006; Wieder et al., 2015). Consequently, more and more models have implemented mechanistic representation of the N cycle in recent decades (Gerber et al., 2010; Goll et al., 2012; Thornton et al., 2007; Wang et al., 2010; Wang et al., 2018; Zaehle & Friend, 2010), and some of them have also incorporated the P cycle (Goll et al., 2012; Wang et al., 2010, 2018; Zhu et al., 2019). In the ongoing Sixth Phase of the Coupled Model Intercomparison Project (CMIP6, Eyring et al., 2016), more than half of the models explicitly represent the N limitation on the terrestrial C cycle (Arora et al., 2020; Davies-Barnard et al., 2020; Jones et al., 2016). These achievements have paved the way to study how N and P cycles interactively and independently affect the global terrestrial C cycle. We thus take advantage of the C-N-P-coupled model to explore whether and how N and P limitations would change the disequilibrium magnitude of the terrestrial C cycle.

In this study, we first provided a theoretical framework to trace factors determining the disequilibrium magnitude of the terrestrial C cycle. Specifically, we separated the dynamic of disequilibrium magnitude into changes in the steady-state C storage and the transit C storage. The steady-state C storage is further decomposed into a productivity-driven change, a  $\tau_E$ -driven change, and a change induced by productivity- $\tau_E$  interactions. Then, we applied the framework with the Australian Community Atmosphere Biosphere Land Exchanges (CABLE) model, which is the land module of the Australian Community Climate and Earth System Simulator (ACCESS-ESM1, Law et al., 2017). The major aim of this study is to use global model simulations with (i.e., C-N and C-N-P) and without (i.e., C-only) nutrient cycles to explore the impacts of nutrient limitation on the disequilibrium magnitude of the terrestrial C cycle.

## 2. Material and Methods

### 2.1. Transient C Cycle Framework

The terrestrial C cycle initiates from photosynthesis through which plants assimilate C from the atmosphere for the growth of leaf, root, and wood. Part of the sequestered C is released back to the atmosphere through autotrophic respiration. Dead tissues of plants are further decomposed and transformed into soil inorganic matter (SOM). Throughout the decomposition processes, some C is consumed and respired by microbes. These C processes determine the dynamics of terrestrial C storage ( $\frac{dX(t)}{dt}$ ), which can be tracked by the below equation (Huang et al., 2018; Luo et al., 2003, 2017; Luo & Weng, 2011; Xia et al., 2013):

$$\frac{dX(t)}{dt} = Bu(t) - AK\xi(t)X(t) \quad (1)$$

where the  $X(t)$  is a vector representing C stocks of different C pools at time  $t$ . The  $u$  is C inputs from photosynthesis (i.e., net primary productivity (NPP)), and the  $B$  is a vector representing the partitioning coefficients of  $u$ . The first term,  $Bu(t)$ , thus represents the partition of photosynthate among different live C pools (e.g., leaf, wood, and root). The second term,  $AK\xi(t)X(t)$ , describes the movements and exit rates of C atoms along their transferring paths (Huang et al., 2018; Luo et al., 2017; Xia et al., 2013). The  $A$ ,  $K$ , and  $\xi$  are all matrices. The  $A$  is a transfer coefficient matrix, representing movements of C atoms among multiple C pools. The  $K$  matrix represents the exit rates of different C pools. The  $\xi$  matrix represents the scalars of environmental factors, such as temperature, moisture, and nutrients.

The C cycle of a terrestrial ecosystem intrinsically tends to chase its steady state over a chronic time frame (Keenan & Williams, 2018; Luo & Weng, 2011). When terrestrial C reservoirs reach their maximum storage capacity at a steady state, there are no further net C exchanges (Luo & Weng, 2011). Therefore, the maximum C storage capacity can be solved by letting Equation 1 equal 0 ( $dX(t)/dt = 0$ ):

$$X_{ss}(t) = (AK\xi(t))^{-1}Bu(t) \quad (2)$$

where  $X_{ss}(t)$  is a vector representing the C storage capacity of different C pools in the steady-state condition (Luo et al., 2017; Xia et al., 2013). The term,  $(AK\xi(t))^{-1}B$ , is a vector that measures the C residence time ( $\tau$ ) of different C pools. The sum of components in the vector is the ecosystem C residence time ( $\tau_E$ ), which is an important ecosystem property involving multiple processes (Carvalhais et al., 2014), including C allocation (the  $B$  vector), C transferring network (the  $A$  matrix), decomposition processes (the  $K$  matrix), and regulations from environmental factors (the  $\xi$  matrix). When considering the NPP as C inputs into an ecosystem, its total C storage capacity  $X_c$  (the sum of components in the vector  $X_{ss}$ ) can thus be defined as

$$X_c(t) = NPP(t) \times \tau_E(t) \quad (3)$$

Under global changes, the terrestrial C cycle is in dynamic disequilibrium (Luo et al., 2017; Luo & Weng, 2011), where the C storage of an ecosystem is perturbed away from its steady-state storage capacity. The difference between the C storage capacity and the current C storage measures the disequilibrium magnitude of the ecosystem ( $X_p$ ):

$$X_p(t) = X_c(t) - X(t) \quad (4)$$

The concept of  $X_p$  is first brought up by Luo et al. (2017). Originally, the  $X_p$  is termed as “C storage potential,” which is conceptually equivalent to the disequilibrium magnitude of the terrestrial C cycle (Luo et al., 2017; Luo & Weng, 2011). To avoid confusion, we define the  $X_p$  as “the disequilibrium magnitude of the terrestrial C cycle” in this study. It should be noted that  $X_c$ ,  $X$ , and  $X_p$  are time-dependent, varying with changes in environmental conditions. Because  $X$  is striving to chase  $X_c$  over time, when  $X$  is smaller than  $X_c$  ( $X_p > 0$ ), ecosystem C storage is expected to increase. Conversely, C losses will happen if  $X$  is larger than  $X_c$  ( $X_p < 0$ ).

## 2.2. Separate Controls on Changes in Disequilibrium Magnitude

The changes in disequilibrium magnitude of terrestrial C cycle over a specific period ( $\Delta X_p$ ) can thus be quantified based on the Equation 4:

$$\Delta X_p = \Delta X_c - \Delta X \quad (5)$$

where the  $\Delta X_c$  represents changes in C storage capacity over that period. The  $\Delta X$  describes changes in the terrestrial C storage. Given  $X_c$  is codetermined by NPP and  $\tau_E$  (Equation 3),  $\Delta X_c$  can thus be estimated by

$$\Delta X_c = NPP(t)\tau_E(t) - NPP_0\tau_{E0} \quad (6)$$

where the  $NPP(t)\tau_E(t)$  represents C storage capacity at the end of the period and  $NPP_0\tau_{E0}$  represents the initial C storage capacity. In order to investigate how changes in C inputs and residence time would influence  $\Delta X_c$ , Equation 6 can be rearranged as

$$\Delta X_c = (NPP_0 + \Delta NPP) \times (\tau_{E0} + \Delta\tau_E) - NPP_0\tau_{E0} \quad (7)$$

$$\Delta X_c = NPP_0\Delta\tau_E + \tau_{E0}\Delta NPP + \Delta\tau_E\Delta NPP \quad (8)$$

where  $NPP_0$  and  $\tau_{E0}$  are the initial values of NPP and  $\tau_E$ , respectively.  $\Delta NPP$  and  $\Delta\tau_E$  are changes in NPP and  $\tau_E$  relative to their initial values. By further combining Equation 8 with Equation 5, the changes in the disequilibrium magnitude of the ecosystem C cycle can be represented by  $\Delta X_p$  as

$$\Delta X_p = NPP_0\Delta\tau_E + \tau_{E0}\Delta NPP + \Delta\tau_E\Delta NPP - \Delta X \quad (9)$$

On the right side of Equation 9, the first term represents changes in C storage capacity rising from changes in  $\tau_E$ . In this term,  $\tau_E$  changes over time, while NPP is held constant at the initial value, which measures  $\tau_E$ -driven changes in  $X_c$  but excludes the influence of changes in  $\tau_E$  on NPP. Similarly, the second term represents NPP-driven changes in  $X_c$ , excluding the influence of changes in NPP on  $\tau_E$ , while the third term represents changes in C storage capacity, resulting from the interactions between NPP and  $\tau_E$ . The last term represents the changes in transient C stock.

## 2.3. Model Description and Experimental Design

The Australian Community Atmosphere Biosphere Land Exchange (CABLE) model (version 2) was applied to conduct the abovementioned mathematical analysis. CABLE is one of the land-surface models, which has fully coupled C, N, and P cycles to simulate land-atmosphere exchange of water, energy, and gases (Wang et al., 2010; Zhang et al., 2011). The structure of the terrestrial C cycle in the CABLE model is shown in Figure S1 of Supporting Information S1. There are 9 C pools in the CABLE model, including leaf, root, wood, metabolic litter, structural litter, coarse woody debris, fast SOM, slow SOM, and passive SOM. Detailed information about converting the modeled land C cycle into the matrix form is provided in the Supporting Information S1.

In the CABLE model, nutrient limitation occurs when the nutrient supply cannot meet the minimal plant demand. Nutrient availability influences terrestrial C sequestration by downregulating photosynthesis, altering allocation patterns, and controlling the decomposition processes (Fleischer, Rammig, et al., 2019; Wang et al., 2010; Wei et al., 2019). For the minimal plant demand on N, it is calculated as the product of maximum N:C ratio and NPP minus resorbed N. The minimal demand on P is modeled similarly as a function of maximum P:C ratio, NPP, and

**Table 1**  
*Data-Model Comparison on the Global Terrestrial Carbon (C) Fluxes and Stocks in the 2000s*

Variables	C-only	CN	CNP	Observation-based estimates
GPP	180	141	137	112.4 <sup>a</sup> ; 135.9 <sup>b</sup>
NPP	90.6	56.5	52.6	58.5 <sup>c</sup> ; 52.3 <sup>d</sup> ays; 44.4 <sup>e</sup>
NEE	-5.2	-2.0	-1.7	-2.6 ± 0.5 <sup>f</sup>
Plant C storage	1,038	554	514	412.3 ± 227 <sup>g</sup>
Soil C storage	2,479	1,336	1,179	1,873 (1,332–2,195) <sup>h–j</sup>

Note. The C fluxes are estimated as the 2001–2010 means in the unit of Pg C yr<sup>-1</sup>. The C stocks are estimated as the size of C storage at the end of 2000s in the unit of Pg C.

<sup>a</sup>FLUXCOM (Jung et al., 2017). <sup>b</sup>VPM (Zhang et al., 2017). <sup>c</sup>MODIS17A2 (Running et al., 2015). <sup>d</sup>CARDAMOM (Bloom et al., 2016). <sup>e</sup>GIMMS-NPP (Kolby Smith et al., 2016). <sup>f</sup>Global carbon budget 2021 (Friedlingstein et al., 2021). <sup>g</sup>Spawn et al., 2020. <sup>h</sup>SoilGrids (Hengl et al., 2017). <sup>i</sup>LandGIS (<https://zenodo.org/record/2536040#.XhxHRBf0kUF>). <sup>j</sup>HWSD V1.2 (Wieder, 2014).

resorbed P. Available nutrients for plant uptake depend on the dynamic of the soil mineral N pool and the soil labile P pool.

Nutrient availability is determined by multiple processes regulating nutrient inputs and outputs (Zaehle & Dalmonech, 2011). In the CABLE model, processes leading to increased N inputs include N deposition (from forcing data), N fixation, and mineralization (Wang et al., 2010). Depletion in available N can result from immobilization, gaseous losses, and N leaching. Gaseous N losses are modeled proportionally to net mineralization, while N leaching is assumed to be proportional to the soil mineral N pool size (Wang et al., 2010). Given that the separation of NH<sub>4</sub><sup>+</sup> and NO<sub>3</sub><sup>-</sup> is not represented in the CABLE model, nitrification and denitrification processes are not explicitly modeled, and ammonia volatilization is not included when modeling N losses.

Soil labile P can be gained from biological and biochemical P mineralization. Biological P mineralization happens along with the mineralization of soil organic matter and is calculated based on the P:C ratio and the C decomposition rate of that pool (Wang et al., 2010). Biochemical P mineralization is modeled as a function of the pool size of soil organic P, the N cost for phosphatase production and P uptake, and the maximal specific biochemical P mineralization rate (Wang et al., 2007). Additionally, P inputs from weathering and atmospheric deposition are directly added to the soil labile P pool. Depletions in the labile P pool are mainly from leaching losses (Wang et al., 2010).

Meteorological data (temperature, precipitation, downward shortwave radiation, downward longwave radiation, specific humidity, pressure, and wind speed) from CRU-NCEP (New et al., 1999, 2000) and observed atmospheric CO<sub>2</sub> concentration data from 1901 to 2013 (Keeling & Whorf, 2005) were used to force CABLE model at a 1° × 1° resolution. The CABLE model in C-only, C-N, and C-N-P modes was spun up separately to approach their steady states in 1901, where X<sub>p</sub> equals zero. The semi-analytical solution method was used to accelerate the spin-up (Xia et al., 2012). Then, we undertook three sets of experiments (C-only, C-N, and C-N-P) from 1901 to 2013 to estimate the effects of incorporating nutrients cycle on ΔX<sub>p</sub> (the difference in mean X<sub>p</sub> between 2004–2013 and 1901–1910). Our study did not consider influences from anthropogenic land use and land cover change (LULCC). The N deposition rate was specified at 1990s levels and kept constant over the simulated period (Wang et al., 2010). Variables needed for the above analysis on ΔX<sub>p</sub> were outputted under the three sets of experiments. The C-only simulation is considered as the baseline. We used the C-N simulation minus the C-only simulation to assess N limitation on ΔX<sub>p</sub> and the C-N-P simulation minus the C-N simulation to assess the P limitation on ΔX<sub>p</sub>.

### 3. Results

#### 3.1. Evaluating Model Performance in Simulating Global Terrestrial C Cycle

We first conducted a data-model comparison on terrestrial C stocks and fluxes to evaluate the performance of the CABLE model in the terrestrial C cycle. In general, the CABLE model in C-N and C-N-P configurations could capture the global terrestrial C cycle in the 2000s (Table 1). The modeled mean GPP over 2001–2010 was 141 Pg C yr<sup>-1</sup> in the C-N configuration, which was slightly larger than the observation-based estimates (112.4–135.9 Pg C yr<sup>-1</sup>). The modeled GPP (137 Pg C yr<sup>-1</sup>) in the C-N-P mode was close to the range derived from data products. The modeled NPP and net ecosystem exchange under CN and CNP runs fell within the range of observation-based estimates. The magnitude of modeled global plant C storage under the C-N and C-N-P coupling schemes matched with the estimates derived from data products (Table 1). The modeled soil C storage under the C-N configuration (1,336 Pg C) was within the observation-based estimates (1,332–2,195 Pg C). The modeled soil C storage in the CNP run was 1,179 Pg C slightly smaller than the range derived from data products. In the C-only mode, the CABLE model overestimated both terrestrial C stocks and fluxes in the 2000s (Table 1).

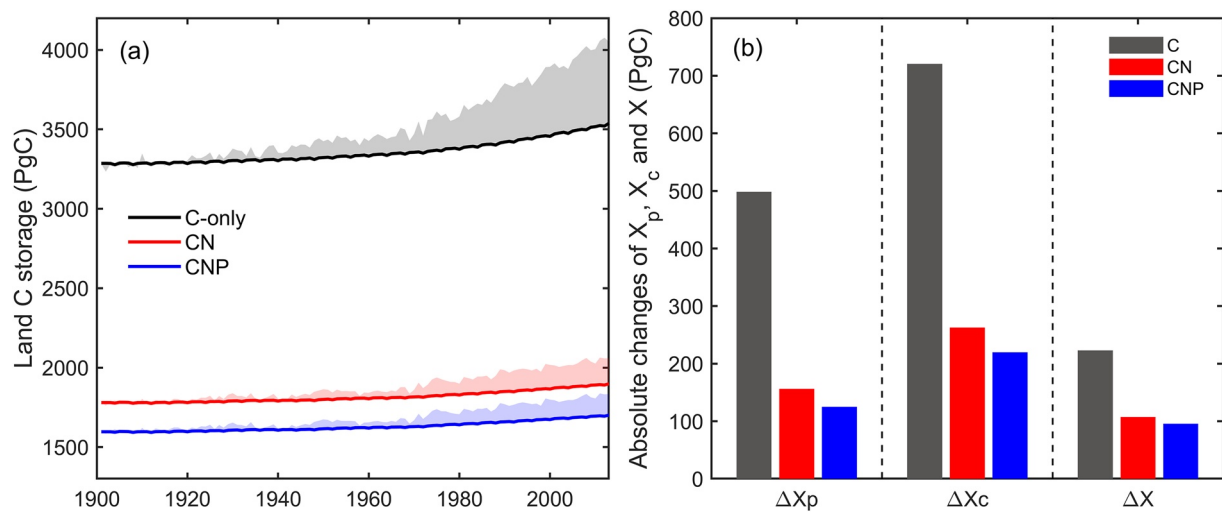


**Figure 1.** (a) The time series of global terrestrial carbon (C) storage capacity ( $X_c$ ) and C storage ( $X$ ) from 1901 to 2013 under C-only, C-N, and C-N-P coupling schemes. The shaded outlines show the time series of annual  $X_c$  and the solid lines show the annual  $X$ . The shaded areas indicate the disequilibrium magnitude ( $X_p$ ), which is estimated as the difference between  $X_c$  and  $X$ . (b) Absolute changes in  $X_p$ ,  $X_c$ , and  $X$  under three different coupling schemes over the modeled period, estimating as the difference between 2004–2013 means and 1901–1910 means.

### 3.2. Nutrient Limitation on the Disequilibrium Magnitude of the Terrestrial C Cycle

Nutrient limitation remarkably reduced the initial states of terrestrial C storage ( $X$ ) and C storage capacity ( $X_c$ , Figure 1). Under the C-only simulation, the initial values of  $X_c$  and  $X$  were 3,286 Pg C (Figure 1a,  $X_c = X$  at the steady state,  $X_p = 0$ ). Considering limitations from N and NP led to 46.1% and 51.4% reductions, respectively, of the initial value of  $X$ . Without nutrient limitation, the terrestrial ecosystem accumulatively sequestered 222.1 Pg C ( $\Delta X$ ) over the modeled period (Figure 1b), while the accumulation of C storage capacity ( $\Delta X_c$ ) was more than threefold larger (719.7 Pg C, Figure 1b). As a result, the magnitude of disequilibrium increased to 497.6 Pg C from 1901 to 2013 (Figure 1b,  $\Delta X_p = \Delta X_c - \Delta X$ ). Once nutrient limitation from N was considered,  $\Delta X_c$  and  $\Delta X$  decreased to 262.1 Pg C and 106.5 Pg C, respectively, which resulted in a far smaller  $\Delta X_p$  (155.6 Pg C) compared with that in the C-only simulation (Figure 1b). Further incorporation of the P cycle with the C-N cycle led to relatively small impacts on  $\Delta X_c$ ,  $\Delta X$ , and  $\Delta X_p$  (Figure 1).

Although three biogeochemical interactions (C-only, C-N, and C-N-P) consistently showed that  $\Delta X_p$  was positive at a global scale over the period of 1901–2013 (Figure 1b), some regions had negative  $\Delta X_p$  under nutrient limitations, such as the subtropical desert in Africa, parts of Europe, and parts of Australia (Figures 2b and 2c). In these regions,  $\Delta X_c$  was smaller than  $\Delta X$ , which indicated a high potential of C losses in the future. The latitudinal pattern under the C-only simulation showed that the northern high-latitude areas had the highest  $\Delta X_p$  than any other place, whereas profound reductions in  $\Delta X_p$  were detected over these regions once nutrient limitation was incorporated (Figure 2d). Nutrient limitations weakened  $\Delta X_p$  by affecting both the  $\Delta X_c$  and the  $\Delta X$  (Figures 1 and 2). However, the spatial patterns of  $\Delta X_p$  under three different biogeochemical interactions all showed good agreement with those of  $\Delta X_c$  (Figures 2a–2h), which indicate the determinative role of  $\Delta X_c$  for  $\Delta X_p$ . We thus further separated controls on  $\Delta X_c$  into three components, as shown in Figure 3, to understand the underlying mechanisms governing the magnitude of  $\Delta X_c$ .

### 3.3. Evaluation of Controls on $\Delta X_c$ Under Nutrient Limitations

Among these components, the NPP-driven term ( $\tau_{E0} \Delta NPP$ ) was the primary factor controlling the magnitude of  $\Delta X_c$  over the modeled period (Figure 3). For the C-only run, the NPP-driven change in the global terrestrial C storage capacity was 694.2 Pg C (Figure 3a), accounting for 96.3% of the  $\Delta X_c$ . Without nutrient limitation, the deciduous needle leaf forest (DNF) showed significant NPP-driven changes in  $X_c$  (Figure 3a and Figure 4a). Due to the long initial ecosystem residence time (584 years) in DNF, even a small change in NPP ( $0.054 \text{ kgC m}^{-2} \text{ year}^{-1}$ ) could lead to huge impacts on equilibrium C storage change (Figure 4b). The situation in the evergreen broadleaf

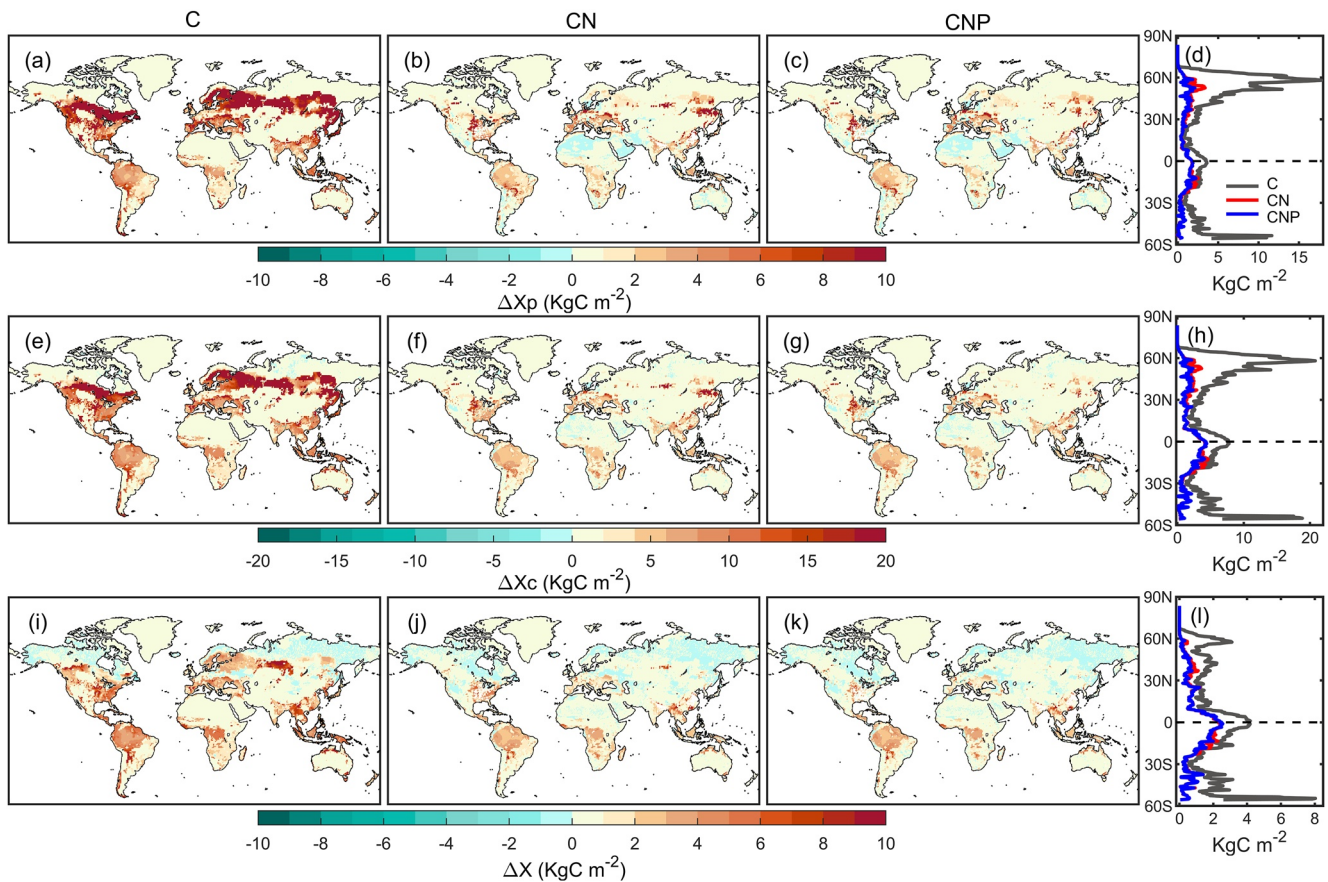


**Figure 2.** The spatial distributions of net change in the magnitude of disequilibrium ( $\Delta X_p$ ), carbon (C) storage capacity ( $\Delta X_c$ ), and ecosystem C storage ( $\Delta X$ ) over the period of 1901–2013, which are estimated by subtracting values at the end of the period (2004–2013 mean) from the initial values (1901–1910 mean) for C-only (a, e, i), C-N (b, f, j), and C-N-P (c, g, k) coupling schemes. Zonal mean plots under three coupling schemes are shown in (d), (h), and (l).

forest (EBF) was different from that in DNF. Over the EBF region, NPP-driven changes in  $X_c$  were mainly a result of changes in NPP ( $0.28 \text{ kg C m}^{-2} \text{ year}^{-1}$ ), while the initial ecosystem residence time was relatively short (30.3 years, Figure 4b). Although the DNF had the largest  $\Delta X_c$  than other biomes (Figures 5a and 5c), the realized terrestrial C sequestration was small ( $\Delta X = 2.04 \text{ KgC m}^{-2}$ , Figure S8 in Supporting Information S1) in comparison with evergreen needle leaf forest (ENF) ( $3.01 \text{ KgC m}^{-2}$ ), EBF ( $5.09 \text{ KgC m}^{-2}$ ), and deciduous broadleaf forest (DBF) ( $4.61 \text{ KgC m}^{-2}$ ). The large unachieved C sequestration in DNF was primarily because its  $\Delta X_p$  was large, accounting for 92.2% of the  $\Delta X_c$  (Figure S7 in Supporting Information S1). If the external climate condition keeps constant over an enough long period, the large  $\Delta X_p$  in DNF can be achieved.

Reductions in  $\tau_{E0}\Delta NPP$  accounted for 94.7% and 94.9% of the reductions in  $\Delta X_c$  under N and NP limitations, respectively (Figure 3). For the CN run, except for the C4 grassland (C4G), all biomes included in our analysis showed shrinking in  $\tau_{E0}\Delta NPP$  (Figure 4a). In comparison with the CN run, reductions in  $\tau_{E0}\Delta NPP$  by further incorporating feedbacks from the P cycle (the CNP run) were minor for all biomes (Figure 4a). Globally, N limitation resulted in a 48.6% reduction in  $\Delta NPP$  and shortened the  $\tau_{E0}$  by 3.2% (Figure 4b). P limitation (CNP—CN) only slightly reduced  $\Delta NPP$  and had hardly effects on  $\tau_{E0}$  (Figure 4b).

### 3.4. Nutrient Limitation on Disequilibrium Magnitude in Plant and Soil C Pools

Over the modeled period,  $\Delta X_p$  in the plant C pool was far smaller than that in the soil C pool under the three configurating schemes (Figure 5). Without nutrient limitation, the  $\Delta X_p$  in plant and soil C pools was  $66.9 \text{ Pg C}$

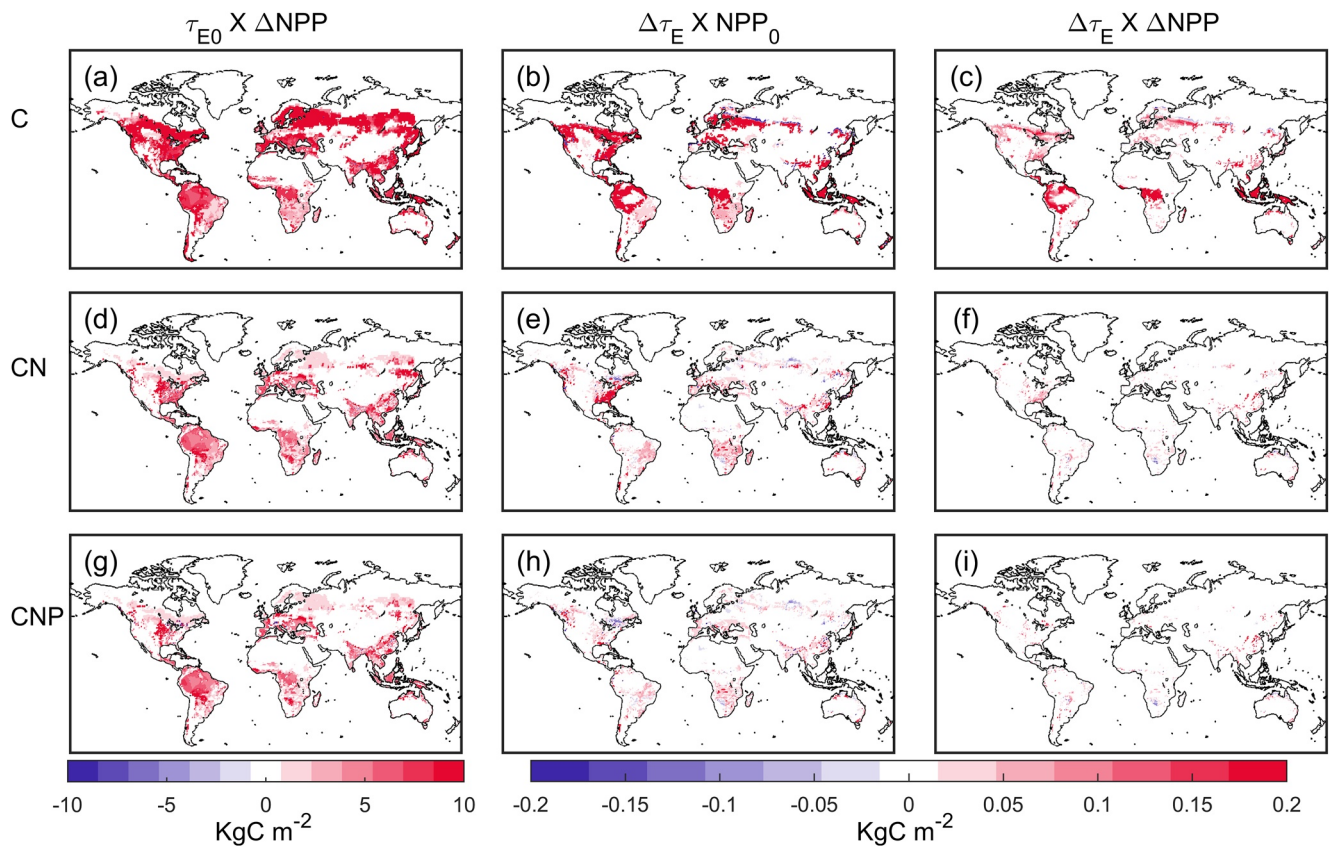


**Figure 3.** Comparison of three determinative components of  $\Delta X_c$  under three biogeochemical interactions. The first and second columns show the net primary productivity (NPP)-driven change and the  $\tau_E$ -driven change in land carbon (C) storage capacity. The third column shows changes in C storage capacity resulted from interactions between NPP and  $\tau_E$ .

and 430.7 Pg C, respectively, at the global scale over 1901–2013 (Figure 5). The  $\Delta X_p$  in plant C pool decreased to 64.3% under N limitation and to 66.8% under NP limitation. Meanwhile,  $\Delta X_p$  in soil C pool reduced to 69.4% and 76.3% under N and NP limitations, respectively. Nutrient limitations also changed the spatial distributions of  $\Delta X_p$  in plant and soil C pools. For the C-only run,  $\Delta X_p$  over tropical and boreal regions was positive and relatively

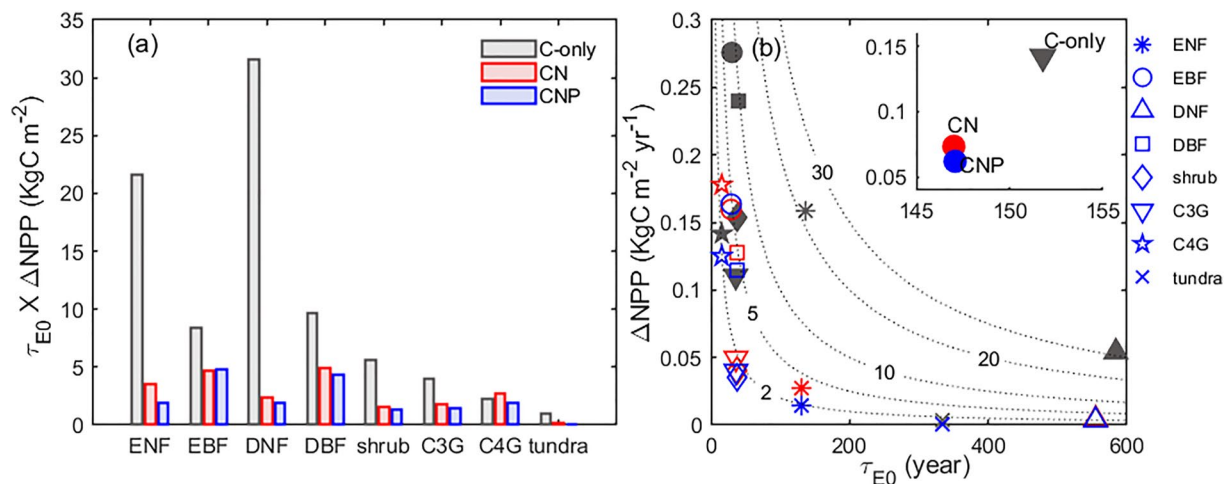


**Figure 4.** (a) Net primary productivity (NPP)-driven change ( $\tau_{E0}\Delta NPP$ ) in  $X_c$  for different biomes over the period of 1901–2013. (b) Net changes in NPP versus initial residence time (1901–1920 mean) in different biomes under three coupling schemes. Details for the abbreviations: ENF-evergreen needle leaf forest, EBF-evergreen broadleaf forest, DNF-deciduous needle leaf forest, DBF-deciduous broadleaf forest, shrub-shrub land, C3G-C<sub>3</sub> grassland, and C4G-C<sub>4</sub> grassland.

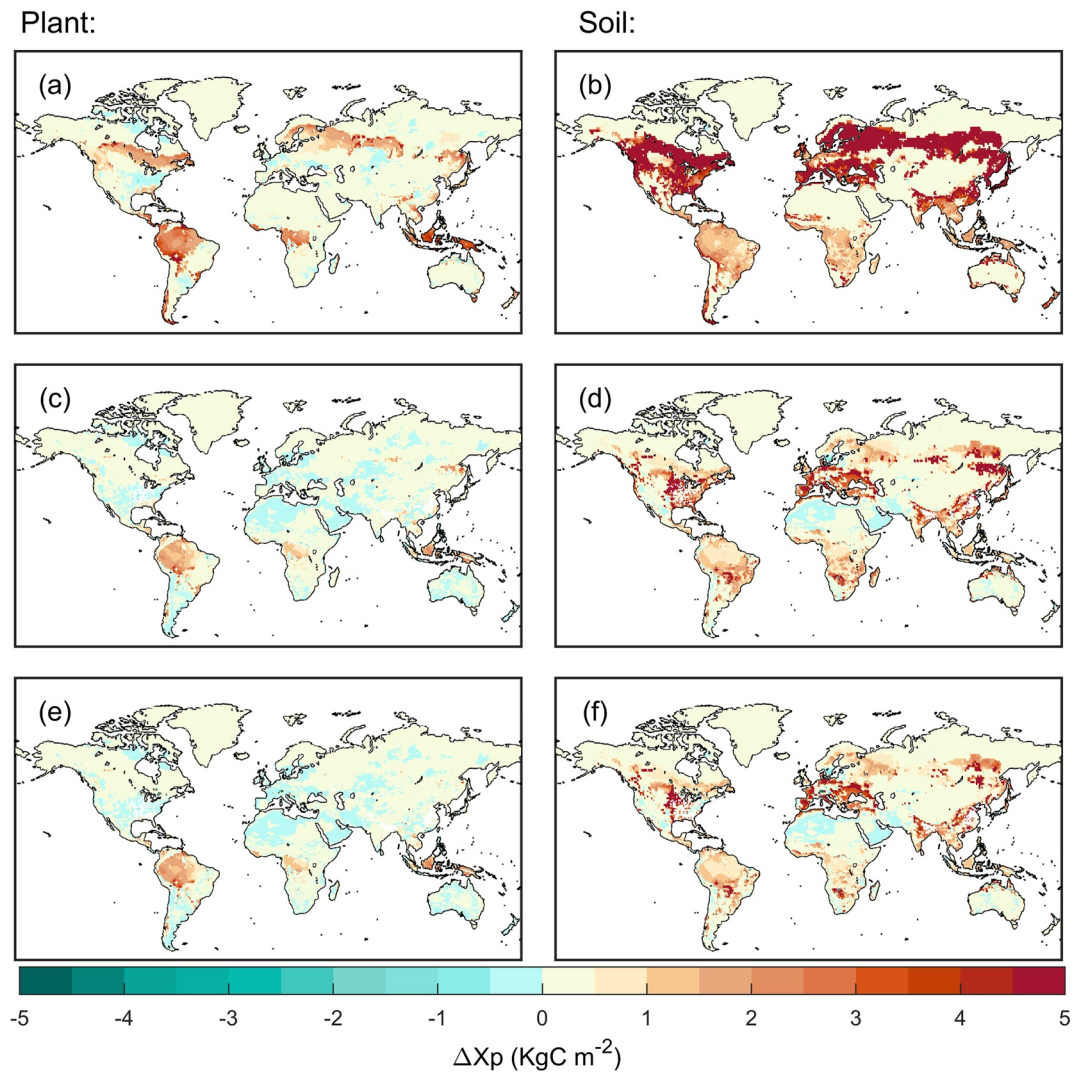


**Figure 5.** The spatial distributions of  $\Delta X_p$  in plant and soil carbon (C) stocks over the period of 1901–2013. The first row of the maps shows condition under the C-only simulation. The second and third rows are for the C-N and C-N-P coupling schemes, respectively.

large compared with other regions (Figures 5a and 5b). When N limitation was considered, reductions of  $\Delta X_p$  in plant and soil C pools were detected globally (Figures 5c and 5d), especially over boreal regions (Figure 5). In comparison with N limitation, the impacts of P limitation on  $\Delta X_p$  were far smaller in both plant and soil C pools.

The large  $\Delta X_p$  in the soil C pool was primarily because it had large  $\Delta X_c$  but relatively small  $\Delta X$  over the modeled period (Figure 6). Under the C-only simulation, the  $\Delta X_c$  in the plant C pool was 187.5 Pg C (Figure 6a). The  $\Delta X_c$  in soil C pool (532.1 Pg C) was nearly threefold larger than that in plant C pool (Figure 6b). However, the  $\Delta X$  in the plant C pool (120.6 Pg C) was larger than that in the soil C pool (101.4 Pg C, Figure 6). Nutrient limitation shrank  $\Delta X_p$  in plant and soil C pools mainly by reducing the  $\tau_{E0}\Delta NPP$ , which was the dominant component driving the equilibrium C storage change in both the plant and soil C pools (Figure 6). In the soil C pool, considering N and NP limitations caused negative  $\Delta\tau_{E'}$ , thus leading to negative  $NPP_0\Delta\tau_{E'}$  and  $\Delta\tau_{E'}\Delta NPP$  (Figure 6c).

For both plant and soil C pools, the  $\tau_{E0}\Delta NPP$  was the dominant component for  $\Delta X_c$  at the global scale (Figure 6). However, the spatial distributions of  $\tau_{E0}\Delta NPP$  for plant (Figure 7) and soil (Figure 8) C pools were different. Without nutrient limitations, most of the  $\tau_{E0}\Delta NPP$  in soil C pool located in boreal regions, while the plant C pool

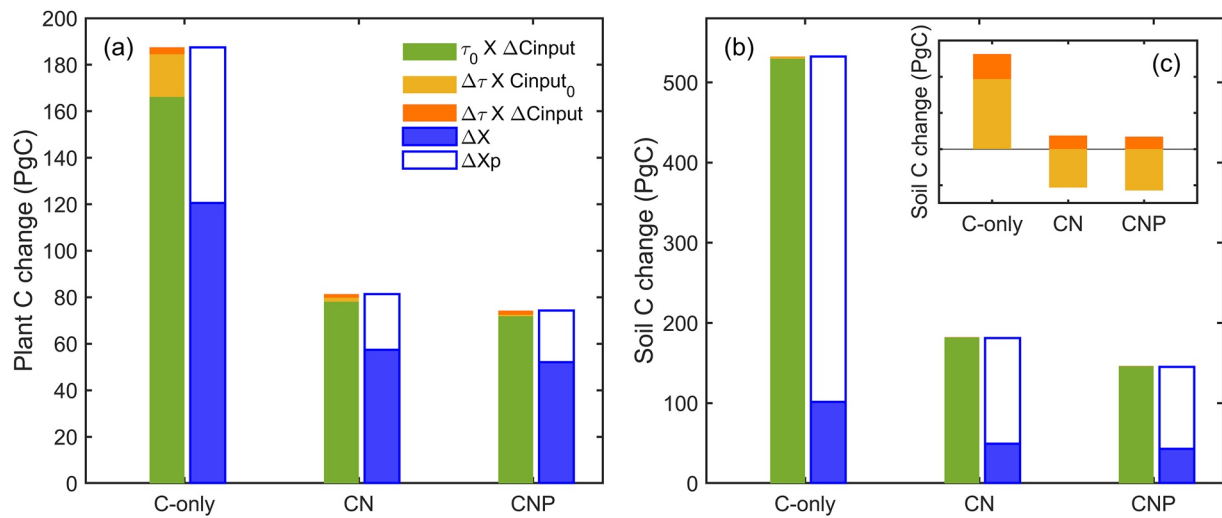


**Figure 6.** Separating controls on  $\Delta X_p$  in plant (a) and soil (b) carbon (C) stocks under three biogeochemical interactions. The first stacked color bar shows three components determining  $\Delta X_c$ . The second one shows  $\Delta X$  and  $\Delta X_p$ . The inserted panel (c) shows changes in C storage driven by changes in residence time and the interactions between C inputs and C residence time.

showed larger  $\tau_{E0}\Delta NPP$  over the tropical region than the boreal region. Incorporating nutrient limitation reduced the  $\tau_{E0}\Delta NPP$  in soil C pool globally, especially profound over the boreal region. For the plant C pool (Figure 8), nutrient limitations almost eliminated the  $\tau_{E0}\Delta NPP$  over the boreal region and greatly reduced the  $\tau_{E0}\Delta NPP$  over the tropical region (Figure 7).

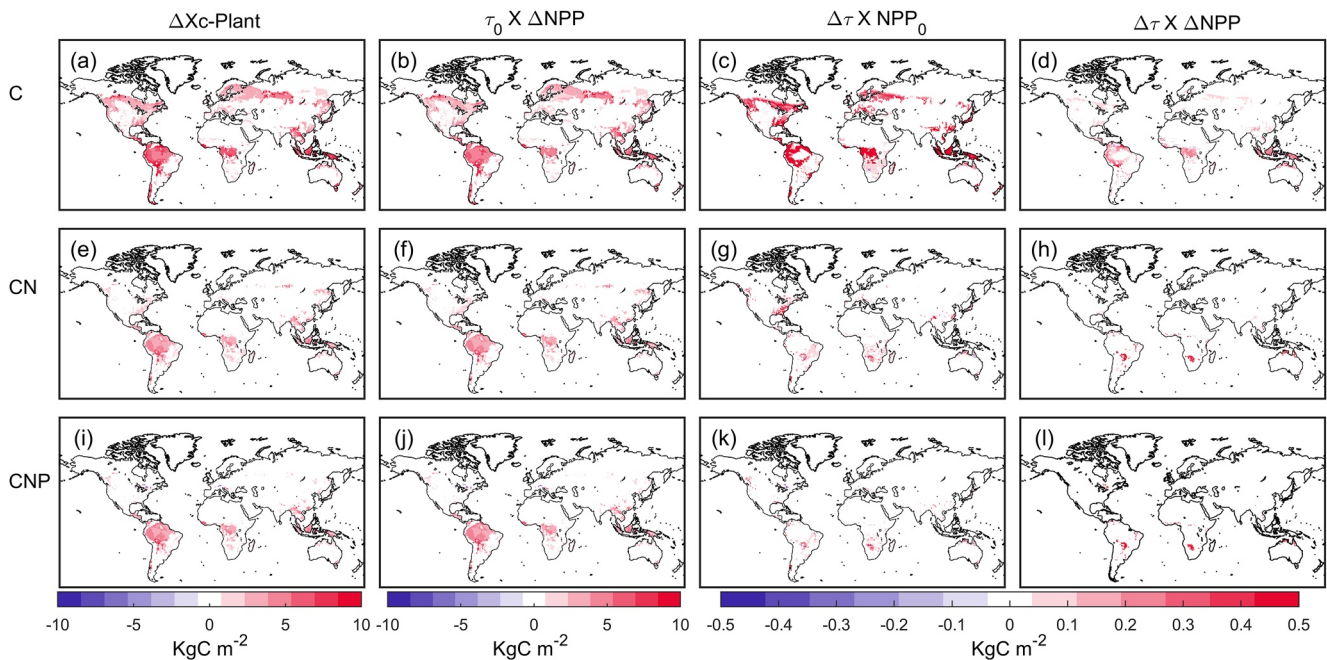


**Figure 7.** The spatial patterns of  $\Delta X_c$  in plant and its three determinants over the period of 1901–2013. The first column represents  $\Delta X_c$  in the plant carbon (C) pool under three biogeochemical interactions. The second and third columns show changes in  $X_c$  driven by changes in C residence time and net primary productivity (NPP), respectively. The last column shows changes in  $X_c$  resulted from co-changes in both NPP and C residence time.

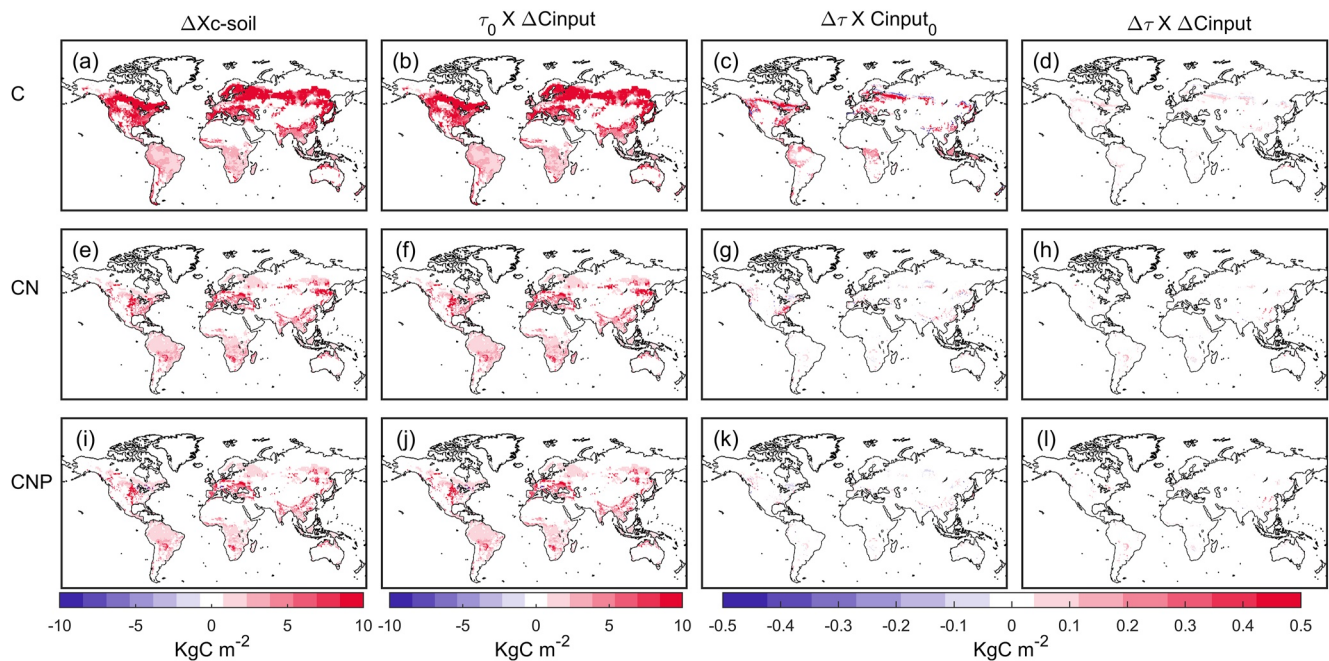


**Figure 8.** The spatial patterns of  $\Delta X_c$  in soil and its three determinants over the period of 1901–2013. The first column represents  $\Delta X_c$  in the soil carbon (C) pool under three biogeochemical interactions. The second and third columns show changes in  $X_c$  driven by changes in C residence time and C input from plant, respectively. The last column shows changes in  $X_c$  resulted from co-changes in both C input into soil and C residence time.

## 4. Discussion

### 4.1. Decrease in $X_p$ Under Nutrient Limitation

The  $X_p$  measures the extent to which the current C storage is away from the steady-state C storage. As an ecosystem tends to chase its steady state (Keenan & Williams, 2018; Luo et al., 2017), the  $X_p$  thus represents the amount of C does not achieve currently. If the same environmental conditions persist for a long time, however, the amount of unachieved C could be attained (Keenan & Williams, 2018; Luo et al., 2017; Luo & Weng, 2011). In our analysis, we find that the  $X_p$  increases considerably over the modeled period without nutrient limitation (Figure 1), whereas the magnitude of its increase is constrained under the N and NP limitations (Figure 1 and Figure 2). If the current environmental conditions keep constant to an infinite time, the constrained increase in  $X_p$  indicates that nutrients limit the attainable C sequestration.

Under transit changes in disturbances and climate, the terrestrial C cycle is in dynamic disequilibrium (Luo et al., 2017; Luo & Weng, 2011). In this study, we disaggregate the changes in disequilibrium magnitude ( $\Delta X_p$ ) into the changes of terrestrial C stocks in equilibrium ( $\Delta X_c$ ) and transit state ( $\Delta X$ , Equation 5). We further show that nutrient limitations will perturb the status of the C cycle, not only lowering the  $\Delta X$ , but also reducing the  $\Delta X_c$ . In the natural ecosystems, the estimate of the disequilibrium magnitude of the terrestrial C cycle could be achieved by applying space-for-time substitution. For example, in an overgrazed grassland, the disequilibrium magnitude of ecosystem C stock can be estimated by measurements with a paired-plot sampling design of proximal plots under overgrazing and without grazing (Conant & Paustian, 2002). The disequilibrium magnitude of the soil C stocks in the overgrazing plot can be approximated as the difference of soil C storage between the undisturbed and overgrazed plots. However, it should be noted that the estimates of the disequilibrium magnitude in C stocks in those empirical studies are generally based on the assumption that historical C losses can be regained with the restoration of the ecosystem (Cannell, 2002; Conant & Paustian, 2002; Lal, 2004).

The quantification of disequilibrium magnitude is also hard in modeling studies due to the high requirement for computation capacity. Consequently, the assumption of a steady state is widely applied in terrestrial C cycle studies (Carvalho et al., 2014; Dybzinski et al., 2015; Koven et al., 2015; Todd-Brown et al., 2013). In these studies, C inputs are assumed to balance against C outputs despite plenty of evidence, suggesting that the terrestrial C

cycle is in a transient state (Lugo & Brown, 1986; Luo & Weng, 2011). Moreover, applying the steady-state assumption can cause biases in both modeling (Carvalhais et al., 2008) and observational studies (Luysaert et al., 2008). When applying the steady-state assumption, future analyses should consider the influences of disequilibrium magnitude on their results (Luo & Weng, 2011).

To understand the underlying mechanism controlling the dynamic of disequilibrium magnitude, we decompose the  $\Delta X_c$  into three components: the NPP-driven change ( $\tau_{E0}\Delta NPP$ ), the  $\tau_E$ -driven change ( $NPP_0\Delta\tau_E$ ), and the NPP- $\tau_E$ -interaction-induced change ( $\Delta\tau_E\Delta NPP$ ) (Equations 8 and 9). Based on a steady-state assumption, many previous studies also separate controls on  $\Delta X_c$  from different aspects (Koven et al., 2015; Taylor & Lloyd, 1992; Todd-Brown et al., 2014; Varney et al., 2020). However, separations in these studies are not comprehensive enough to include all terms shown in Equation 8. For example, effects from changes in NPP and  $\tau_E$  on terrestrial C sink are separated by allowing one factor that varies with time and setting the other constant (Koven et al., 2015; Todd-Brown et al., 2014; Varney et al., 2020). How changes in NPP and  $\tau_E$  interactively ( $\Delta\tau_E\Delta NPP$ ) contribute to  $\Delta X_c$  is rarely considered, which could cause bias in long-term estimations. It is especially the case under the nutrient limitation. Plant NPP is constrained by nutrient availability, and poor-quality litters (high C:N ratio) are yielded, which alter decomposition rate and  $\tau_E$ . The changed  $\tau_E$  could in turn trigger changes in nutrient availability, further affecting NPP. Thus, the NPP- $\tau_E$  interactions will change the  $\Delta X_c$  slowly, and the impacts should not be ignored over a chronic period.

#### 4.2. Nutrient Limitation Reduces $\Delta X_p$ by Constraining NPP-Driven Increases in $X_c$

Over the modeled period of 1901–2013, nutrient limitations reduce  $\Delta X_p$  primarily by constraining NPP-driven ( $\tau_{E0}\Delta NPP$ ) increases in the terrestrial C storage capacity (Figure 3 and Figure 6). To some extent, this pattern agrees with the widely observed nutrient limitations on NPP among biomes (Elser et al., 2007; LeBauer & Treseder, 2008; Norby et al., 2010). In field experiments, the nutrient limitation is generally defined by the stimulated rate of biological processes after adding nutrients (Vitousek et al., 2010). In such a way, terrestrial productivity is widely found to be constrained by N and P availability (Elser et al., 2007; LeBauer & Treseder, 2008). However, based on the nutrient-limited NPP alone, we cannot extrapolate the extent to which the steady-state C storage (Crowther et al., 2019) and the disequilibrium magnitude would be limited by nutrients. Assuming  $\tau_E$  does not significantly change, the same magnitude of reduction in NPP under nutrient limitation could lead to different extent of impacts on  $\Delta X_c$  and  $\Delta X_p$  as shown in Figure 4b. Taking the DNF and ENF as examples, the DNF shows a relatively small reduction in NPP under N limitation compared to ENF. However, the DNF shows severer nutrient constraints on the NPP-driven changes in  $X_c$  than the ENF because the DNF has a larger  $\tau_{E0}$ .

Over the short term, it is not surprising that nutrient limitation strongly reduces the NPP-driven term as photosynthesis and plant growth are sensitive to nutrient availability. Over a chronic period, the  $\tau_E$ -driven term (primarily determined by  $\Delta\tau_E$ ) could turn to influence  $\Delta X_c$  and  $\Delta X_p$  under nutrient limitations (Fleischer, Rammig, et al., 2019). At a global scale, we find that the  $\tau_E$ -driven term ( $NPP_0\Delta\tau_E$ ) is restrained by nutrients (Figure 3), whereas the  $\tau_E$ -driven term makes minor contributions to the  $\Delta X_c$  under three biogeochemical interactions (Figure 3 and Figure 4). The minor contribution of the  $\tau_E$ -driven term is due to the relatively small  $\Delta\tau_E$  over the modeled period (Figure S6 in Supporting Information S1). Note that we calculate  $\tau_E$  based on a bottom-up approach that multiplies all determinative processes using the model's matrix representation (Supporting Information S1). As observations of stocks and fluxes can easily be obtained, many previous studies apply the stock-to-flux ratio (the turnover time) to indicate the time characteristics in the C cycle (Carvalhais et al., 2014; Fleischer, Rammig, et al., 2019; Friend et al., 2014; Koven et al., 2015; Todd-Brown et al., 2013), such that the calculated turnover time is highly dependent on C fluxes. Under nutrient limitation, for example, NPP is more responsive than ecosystem C storage. Thus, the ratio is more changeable over time in comparison with the calculated  $\tau_E$  in our study. Recently, Lu et al. (2018) found that ecosystem C turnover time deviates from residence time under warming and rising atmospheric  $CO_2$  concentration. Under nutrient limitation, it thus needs cautions when using the turnover time to interpret the time characteristics of the C cycle (Wang et al., 2019).

Without nutrient limitations, many regions show slight increases in  $\tau_E$  ( $\Delta\tau_E > 0$ ) over the modeled period (Figure S6 in Supporting Information S1). Considering nutrient limitation diminishes the positive  $\Delta\tau_E$  (Figures S6d and S6f in Supporting Information S1), which results in the negligible effects of both  $NPP_0\Delta\tau_E$  and  $\Delta\tau_E\Delta NPP$  on changes in  $\Delta X_c$  (Figure 3). The  $\Delta\tau_E$  can be explained by how the respired C composition and the compartment C

age structure change (Lu et al., 2018; Rasmussen et al., 2016; Sierra et al., 2017). Previous modeling analysis with the CABLE model shows that climate warming could increase  $\tau_E$  by stimulating the depletion of fast-turnover soil organic C and changing the C age structure (Lu et al., 2018). Raising in atmospheric CO<sub>2</sub> concentration could decrease  $\tau_E$  by increasing C input of a young age (Lu et al., 2018). Insufficient nutrient supply could constrain young C uptake under enrichment in atmospheric CO<sub>2</sub>, which could dampen the decrease in compartment C age structure. On the other hand, the decomposition of soil organic matter is also limited by nutrient availability, slowing down the depletion of fast-turnover soil organic C under climate warming. The two opposite effects might become comparable under nutrient limitations, which leads to the insignificant change in  $\tau_E$  in this study.

### 4.3. Nutrient Limitation on $\Delta X_p$ in Plant and Soil

We also apply the proposed framework to investigate  $\Delta X_p$  in plant and soil C pools, given that relevant processes operate at different time scales for plant and soil. The plant C pool has a smaller  $\Delta X_p$  in comparison with the soil C pool although C accumulation in the plant C pool is larger than that in soil C pool over the modeled period (Figure 6). For the soil C pool, it has a nearly threefold larger C-input-driven (C inputs from plant litter) increase in  $X_c$  than the plant C pool, while its large  $\Delta X_p$  causes a great proportion of C storage capacity to be unattained over the modeled period (Figure 6). These results imply that the potential of plant C pool to increase C sequestration is limited as both the C storage capacity and the magnitude of disequilibrium are relatively small for the plant C pool. In contrast, the disequilibrium magnitude in the soil C pool is large but can be significantly constrained by nutrient availability (Figure 6 and Figure 8). Under nutrient limitations, we detected decreases in soil C residence time (Figure S10 in Supporting Information S1), which might result from acceleration of decomposition to alleviate nutrient limitation on plant growth. To maximize ecosystem C sequestration strength, it thus requires efficient plant-soil feedbacks in C and nutrient cycling over the long term (De Deyn et al., 2008).

Parametric and structural uncertainty related to C-nutrient coupling could affect the estimated magnitude of nutrient limitation on  $\Delta X_p$ . In the CABLE model, parameters determining soil N availability (i.e., N leaching rate) can cause significant variations in  $\Delta X_p$  (Figure S13 in Supporting Information S1). Many previous studies have extensively evaluated uncertainty associated with biogeochemical cycling in the CABLE model (Exbrayat et al., 2013; Lu et al., 2013; Wang et al., 2010, 2011; Xia et al., 2017). Those studies suggest that a lack of flexibility in allocation patterns (Xia et al., 2017), incomplete representation of N fixation (Fisher et al., 2019), and weak interaction between C and P cycles (Fleischer, Rammig, et al., 2019) can together cause uncertainty in the modeled terrestrial C cycle. Furthermore, current C-nutrient coupled models varied widely in representing key processes controlling the dynamics of nutrient cycling and the C-nutrient interactions (Davies-Barnard et al., 2020; Du et al., 2018; Fleischer, Rammig, et al., 2019). For example, some models apply an optimizable plant allocation strategy, whereas others use a fixed allocation ratio (Fleischer, Rammig, et al., 2019). Mechanisms associated with nutrient availability and nutrient acquisition are also differently represented among models (Meyerholt et al., 2020). When applying different C-nutrient-coupled models to investigate the nutrient limitation on disequilibrium magnitude in the terrestrial C cycle, results might differ among models. Although our analysis is based on a single C-N-P-coupled land-surface model, the proposed framework can be generally applied to other models, which could help investigate how changes in NPP,  $\tau_E$ , and land C storage could affect  $\Delta X_p$  in different model assumptions of C-nutrient coupling.

Some other limitations should also be noted. First, the vegetation distribution in CABLE is prescribed (Wang et al., 2010). Thus, changes in terrestrial C sink induced by vegetation dynamics under climate change and rising in atmospheric CO<sub>2</sub> concentration are not involved in our study. Furthermore, human-induced land use and land cover change (LULCC) and changes in atmospheric N deposition are not considered. Including land use and land cover change (LULCC) has been estimated to reduce land C uptake to different degrees (Wang et al., 2015). Deforestation and inappropriate land management could even turn the terrestrial C sink into a source (Wang et al., 2015). We thus speculate that LULCC might change the disequilibrium magnitude from positive to negative over many areas. However, the extent to which N deposition can relieve nutrient limitation on the disequilibrium of the terrestrial C cycle needs further research. Especially, future enhanced N deposition is projected to cause shifts in the spatial pattern of N and P limitations (Fleischer, Dolman, et al., 2019; Peñuelas et al., 2013).

## 5. Conclusion

Overall, we assessed whether and how nutrient limitations from N and P would drive changes in the disequilibrium magnitude of the terrestrial C cycle. We find that nutrient conditions do have impacts on the disequilibrium magnitude. Without sufficient nutrient supply, increases in the disequilibrium magnitude under the stimulation of CO<sub>2</sub> and climate change are largely dampened (Figure S2 in Supporting Information S1). The diminishing disequilibrium magnitude indicates that nutrient limitation affects the current terrestrial C sequestration strength ( $\Delta X$ ) and the capacity of an ecosystem to sequester C from the atmosphere. Over the modeled period, nutrient limitation decreases the  $\Delta X_p$  primarily by dampening NPP-driven increases in the steady-state C storage. The influences from changes in  $\tau_E$  (the  $\tau_E$ -driven term and the NPP- $\tau_E$ -interaction term) are negligible in this study, but might become dominant over a long time period. This study recommends more research efforts to combine the field observations and process-based models to explore the changes in the disequilibrium magnitude of terrestrial C stock in specific ecosystems. Overall, our study underscores the importance of nutrient availability in determining the disequilibrium magnitude of the terrestrial C cycle in a transient state.

## Conflict of Interest

The authors declare no conflicts of interest relevant to this study.

## Data Availability Statement

The codes of the CABLE model can be downloaded from <https://trac.nci.org.au/trac/cable>. The code and meta-data for associated analysis and producing main figures can be accessed from [https://figshare.com/articles/dataset/Nutrient\\_limitations\\_lead\\_to\\_a\\_reduced\\_magnitude\\_of\\_disequilibrium\\_in\\_the\\_global\\_terrestrial\\_carbon\\_cycle/19409639](https://figshare.com/articles/dataset/Nutrient_limitations_lead_to_a_reduced_magnitude_of_disequilibrium_in_the_global_terrestrial_carbon_cycle/19409639).

## Acknowledgments

This work was financially supported by the National Key R&D Program of China (2017YFA0604600) and National Natural Science Foundation of China (31722009 and 41630528).

## References

- Arora, V. K., Katavouta, A., Williams, R. G., Jones, C. D., Brovkin, V., Friedlingstein, P., et al. (2020). Carbon–concentration and carbon–climate feedbacks in CMIP6 models and their comparison to CMIP5 models. *Biogeosciences*, *17*(16), 4173–4222. <https://doi.org/10.5194/bg-17-4173-2020>
- Averill, C., & Waring, B. (2017). Nitrogen limitation of decomposition and decay: How can it occur? *Global Change Biology*, *24*(4), 1417–1427. <https://doi.org/10.1111/gcb.13980>
- Bloom, A. A., Exbrayat, J. F., van der Velde, I. R., Feng, L., & Williams, M. (2016). The decadal state of the terrestrial carbon cycle: Global retrievals of terrestrial carbon allocation, pools, and residence times. *Proceedings of the National Academy of Sciences*, *113*(5), 1285–1290. <https://doi.org/10.1073/pnas.1515160113>
- Canadell, J. G., Le Quere, C., Raupach, M. R., Field, C. B., Buitenhuis, E. T., Ciais, P., et al. (2007). Contributions to accelerating atmospheric CO<sub>2</sub> growth from economic activity, carbon intensity, and efficiency of natural sinks. *Proceedings of the National Academy of Sciences*, *104*(47), 18866–18870. <https://doi.org/10.1073/pnas.0702737104>
- Cannell, M. G. (2002). Carbon sequestration and biomass energy offset: Theoretical, potential and achievable capacities globally, in Europe and the UK. *Biomass and Bioenergy*, *24*(2), 97–116. [https://doi.org/10.1016/s0961-9534\(02\)00103-4](https://doi.org/10.1016/s0961-9534(02)00103-4)
- Carvalho, N., Forkel, M., Khomik, M., Bellarby, J., Jung, M., Migliavacca, M., et al. (2014). Global covariation of carbon turnover times with climate in terrestrial ecosystems. *Nature*, *514*(7521), 213–217. <https://doi.org/10.1038/nature13731>
- Carvalho, N., Reichstein, M., Seixas, J., Collatz, G. J., Pereira, J. S., Berbigier, P., et al. (2008). Implications of the carbon cycle steady state assumption for biogeochemical modeling performance and inverse parameter retrieval. *Global Biogeochemical Cycles*, *22*(2), GB2007. <https://doi.org/10.1029/2007GB003033>
- Conant, R. T., & Paustian, K. (2002). Potential soil carbon sequestration in overgrazed grassland ecosystems. *Global Biogeochemical Cycles*, *16*(4), 901–909. <https://doi.org/10.1029/2001gb001661>
- Crowther, T. W., Riggs, C., Lind, E. M., Borer, E. T., Seabloom, E. W., Hobbie, S. E., et al. (2019). Sensitivity of global soil carbon stocks to combined nutrient enrichment. *Ecology Letters*, *22*(6), 936–945. <https://doi.org/10.1111/ele.13258>
- Davies-Barnard, T., Meyerholt, J., Zaehle, S., Friedlingstein, P., Brovkin, V., Fan, Y., et al. (2020). Nitrogen cycling in CMIP6 land surface models: Progress and limitations. *Biogeosciences*, *17*(20), 5129–5148. <https://doi.org/10.5194/bg-17-5129-2020>
- De Deyn, G. B., Cornelissen, J. H. C., & Bardgett, R. D. (2008). Plant functional traits and soil carbon sequestration in contrasting biomes. *Ecology Letters*, *11*(5), 516–531. <https://doi.org/10.1111/j.1461-0248.2008.01164.x>
- Du, Z., Weng, E., Jiang, L., Luo, Y., Xia, J., & Zhou, X. (2018). Carbon–nitrogen coupling under three schemes of model representation: A traceability analysis. *Geoscientific Model Development*, *11*, 4399–4416. <https://doi.org/10.5194/gmd-11-4399-2018>
- Dybziński, R., Farris, C. E., & Pacala, S. W. (2015). Increased forest carbon storage with increased atmospheric CO<sub>2</sub> despite nitrogen limitation: A game-theoretic allocation model for trees in competition for nitrogen and light. *Global Change Biology*, *21*(3), 1182–1196. <https://doi.org/10.1111/gcb.12783>
- Elser, J. J., Bracken, M. E., Cleland, E. E., Gruner, D. S., Harpole, W. S., Hillebrand, H., et al. (2007). Global analysis of nitrogen and phosphorus limitation of primary producers in freshwater, marine and terrestrial ecosystems. *Ecology Letters*, *10*(12), 1135–1142. <https://doi.org/10.1111/j.1461-0248.2007.01113.x>

- Exbrayat, J. F., Pitman, A. J., Zhang, Q., Abramowitz, G., & Wang, Y. P. (2013). Examining soil carbon uncertainty in a global model: Response of microbial decomposition to temperature, moisture and nutrient limitation. *Biogeosciences*, *10*(11), 7095–7108. <https://doi.org/10.5194/bg-10-7095-2013>
- Eyring, V., Bony, S., Meehl, G. A., Senior, C. A., Stevens, B., Stouffer, R. J., & Taylor, K. E. (2016). Overview of the Coupled Model Inter-comparison Project Phase 6 (CMIP6) experimental design and organization. *Geoscientific Model Development*, *9*(5), 1937–1958. <https://doi.org/10.5194/gmd-9-1937-2016>
- Fisher, J. B., Huntzinger, D. N., Schwalm, C. R., & Sitch, S. (2014). Modeling the Terrestrial Biosphere. *Annual Review of Environment and Resources*, *39*(1), 91–123. <https://doi.org/10.1146/annurev-environ-012913-093456>
- Fisher, R. A., & Koven, C. D. (2020). Perspectives on the future of land surface models and the challenges of representing complex terrestrial systems. *Journal of Advances in Modeling Earth Systems*, *12*(4), e2018MS001453. <https://doi.org/10.1029/2018ms001453>
- Fisher, R. A., Wieder, W. R., Sanderson, B. M., Koven, C. D., Oleson, K. W., Xu, C., et al. (2019). Parametric controls on vegetation responses to biogeochemical forcing in the CLM5. *Journal of Advances in Modeling Earth Systems*, *11*(9), 2879–2895. <https://doi.org/10.1029/2019ms001609>
- Fleischer, K., Dolman, A. J., Molen, M. K., Rebel, K. T., Erisman, J. W., Wassen, M. J., et al. (2019). Nitrogen deposition maintains a positive effect on terrestrial carbon sequestration in the 21st century despite growing phosphorus limitation at regional scales. *Global Biogeochemical Cycles*, *33*(6), 810–824. <https://doi.org/10.1029/2018gb005952>
- Fleischer, K., Rammig, A., De Kauwe, M. G., Walker, A. P., Domingues, T. F., Fuchslueger, L., et al. (2019). Amazon forest response to CO<sub>2</sub> fertilization dependent on plant phosphorus acquisition. *Nature Geoscience*, *12*(9), 736–741. <https://doi.org/10.1038/s41561-019-0404-9>
- Friedlingstein, P., Jones, M. W., O'Sullivan, M., Andrew, R. M., Bakker, D. C., Hauck, J., et al. (2021). Global carbon budget 2021. *Earth System Science Data Sci Data Discussions*. <https://doi.org/10.5194/essd-2021-386>
- Friedlingstein, P., O'Sullivan, M., Jones, M. W., Andrew, R. M., Bakker, D. C., Olsen, A., et al. (2020). Global carbon budget 2020. *Earth System Science Data*, *12*(4), 3269–3340. <https://doi.org/10.5194/essd-12-3269-2020>
- Friend, A. D., Lucht, W., Rademacher, T. T., Keribin, R., Betts, R., Cadule, P., et al. (2014). Carbon residence time dominates uncertainty in terrestrial vegetation responses to future climate and atmospheric CO<sub>2</sub>. *Proceedings of the National Academy of Sciences*, *111*(9), 3280–3285. <https://doi.org/10.1073/pnas.1222477110>
- Gerber, S., Hedin, L. O., Oppenheimer, M., Pacala, S. W., & Shevliakova, E. (2010). Nitrogen cycling and feedbacks in a global dynamic land model. *Global Biogeochemical Cycles*, *24*(1), GB1001. <https://doi.org/10.1029/2008GB003336>
- Goll, D. S., Brovkin, V., Parida, B. R., Reick, C. H., Kattge, J., Reich, P. B., et al. (2012). Nutrient limitation reduces land carbon uptake in simulations with a model of combined carbon, nitrogen and phosphorus cycling. *Biogeosciences*, *9*(9), 3547–3569. <https://doi.org/10.5194/bg-9-3547-2012>
- Hengl, T., Mendes de Jesus, J., Heuvelink, G. B. M., Ruiperez Gonzalez, M., Kilibarda, M., Blagotic, A., et al. (2017). SoilGrids250m: Global gridded soil information based on machine learning. *PLoS One*, *12*(2), e0169748. <https://doi.org/10.1371/journal.pone.0169748>
- Hessen, D. O., Agren, G. I., Anderson, T. R., Elser, J. J., & de Ruiter, P. C. (2004). Carbon sequestration in ecosystems: The role of stoichiometry. *Ecology*, *85*(5), 1179–1192. <https://doi.org/10.1890/02-0251>
- Hofhansl, F., Andersen, K. M., Fleischer, K., Fuchslueger, L., Rammig, A., Schaap, K. J., et al. (2016). Amazon forest ecosystem responses to elevated atmospheric CO<sub>2</sub> and alterations in nutrient availability: Filling the gaps with model-experiment integration. *Frontiers of Earth Science*, *4*(19), 2296–6463. <https://doi.org/10.3389/feart.2016.00019>
- Huang, Y., Lu, X., Shi, Z., Lawrence, D., Koven, C. D., Xia, J., et al. (2018). Matrix approach to land carbon cycle modeling: A case study with the Community Land Model. *Global Change Biology*, *24*(3), 1394–1404. <https://doi.org/10.1111/gcb.13948>
- Huntzinger, D. N., Schwalm, C., Michalak, A. M., Schaefer, K., King, A. W., Wei, Y., et al. (2013). The North American carbon program multi-scale synthesis and terrestrial model intercomparison project – Part 1: Overview and experimental design. *Geoscientific Model Development*, *6*(6), 2121–2133. <https://doi.org/10.5194/gmd-6-2121-2013>
- Jones, C. D., Arora, V., Friedlingstein, P., Bopp, L., Brovkin, V., Dunne, J., et al. (2016). C4MIP – The Coupled Climate–Carbon Cycle Model Intercomparison Project: Experimental protocol for CMIP6. *Geoscientific Model Development*, *9*(8), 2853–2880. <https://doi.org/10.5194/gmd-9-2853-2016>
- Jung, M., Reichstein, M., Schwalm, C. R., Huntingford, C., Sitch, S., Ahlstrom, A., et al. (2017). Compensatory water effects link yearly global land CO<sub>2</sub> sink changes to temperature. *Nature*, *541*(7638), 516–520. <https://doi.org/10.1038/nature20780>
- Keeling, C. D., & Whorf, T. P. (2005). Atmospheric CO<sub>2</sub> records from sites in the SIO air sampling network. In *Trends: A compendium of data on global change* (pp. 16–26).
- Keenan, T. F., & Williams, C. A. (2018). The terrestrial carbon sink. *Annual Review of Environment and Resources*, *43*(1), 219–243. <https://doi.org/10.1146/annurev-environ-102017-030204>
- Kolby Smith, W., Reed, S. C., Cleveland, C. C., Ballantyne, A. P., Anderegg, W. R. L., Wieder, W. R., et al. (2016). Large divergence of satellite and Earth system model estimates of global terrestrial CO<sub>2</sub> fertilization. *Nature Climate Change*, *6*(3), 306–310. <https://doi.org/10.1038/nclimate2879>
- Koven, C. D., Chambers, J. Q., Georgiou, K., Knox, R., Negron-Juarez, R., Riley, W. J., et al. (2015). Controls on terrestrial carbon feedbacks by productivity versus turnover in the CMIP5 Earth System Models. *Biogeosciences*, *12*(17), 5211–5228. <https://doi.org/10.5194/bg-12-5211-2015>
- Lal, R. (2004). Soil carbon sequestration impacts on global climate change and food security. *Science*, *304*(5677), 1623–1627. <https://doi.org/10.1126/science.1097396>
- Law, R. M., Ziehn, T., Matear, R. J., Lenton, A., Chamberlain, M. A., Stevens, L. E., et al. (2017). The carbon cycle in the Australian Community Climate and Earth System Simulator (ACCESS-ESM1) – Part 1: Model description and pre-industrial simulation. *Geoscientific Model Development*, *10*(7), 2567–2590. <https://doi.org/10.5194/gmd-10-2567-2017>
- LeBauer, D. S., & Treseder, K. K. (2008). Nitrogen limitation of net primary productivity in terrestrial ecosystems is globally distributed. *Ecology*, *89*(2), 371–379. <https://doi.org/10.1890/06-2057.1>
- Le Quéré, C., Andrew, R. M., Friedlingstein, P., Sitch, S., Pongratz, J., Manning, A. C., et al. (2018). Global Carbon Budget 2017. *Earth System Science Data*, *10*(1), 405–448.
- Lu, X., Wang, Y. P., Luo, Y., & Jiang, L. (2018). Ecosystem carbon transit versus turnover times in response to climate warming and rising atmospheric CO<sub>2</sub> concentration. *Biogeosciences*, *15*(21), 6559–6572. <https://doi.org/10.5194/bg-15-6559-2018>
- Lu, X., Wang, Y. P., Ziehn, T., & Dai, Y. (2013). An efficient method for global parameter sensitivity analysis and its applications to the Australian community land surface model (CABLE). *Agricultural and Forest Meteorology*, *182*–183, 292–303. <https://doi.org/10.1016/j.agrformet.2013.04.003>

- Lugo, A. E., & Brown, S. (1986). Steady state terrestrial ecosystems and the global carbon cycle. *Vegetatio*, 68(2), 83–90. <https://doi.org/10.1007/bf00045058>
- Luo, Y., Shi, Z., Lu, X., Xia, J., Liang, J., Jiang, J., et al. (2017). Transient dynamics of terrestrial carbon storage: Mathematical foundation and its applications. *Biogeosciences*, 14(1), 145–161. <https://doi.org/10.5194/bg-14-145-2017>
- Luo, Y., & Weng, E. (2011). Dynamic disequilibrium of the terrestrial carbon cycle under global change. *Trends in Ecology & Evolution*, 26(2), 96–104. <https://doi.org/10.1016/j.tree.2010.11.003>
- Luo, Y., White, L. W., Canadell, J. G., DeLucia, E. H., Ellsworth, D. S., Finzi, A., et al. (2003). Sustainability of terrestrial carbon sequestration: A case study in Duke Forest with inversion approach. *Global Biogeochemical Cycles*, 17(1), 1021. <https://doi.org/10.1029/2002GB001923.1>
- Luyssaert, S., Schulze, E. D., Börner, A., Knohl, A., Hessenmoller, D., Law, B. E., et al. (2008). Old-growth forests as global carbon sinks. *Nature*, 455(7210), 213–215. <https://doi.org/10.1038/nature07276>
- Menge, D. N. L., & Field, C. B. (2007). Simulated global changes alter phosphorus demand in annual grassland. *Global Change Biology*, 13(12), 2582–2591. <https://doi.org/10.1111/j.1365-2486.2007.01456.x>
- Meyerholt, J., Sicking, K., & Zaehle, S. (2020). Ensemble projections elucidate effects of uncertainty in terrestrial nitrogen limitation on future carbon uptake. *Global Change Biology*, 26(7), 3978–3996. <https://doi.org/10.1111/gcb.15114>
- New, M., Hulme, M., & Jones, P. (1999). Representing twentieth-century space–time climate variability. Part I: Development of a 1961–90 mean monthly terrestrial climatology. *Journal of Climate*, 12(3), 829–856. [https://doi.org/10.1175/1520-0442\(1999\)012<0829:rtctsc>2.0.co;2](https://doi.org/10.1175/1520-0442(1999)012<0829:rtctsc>2.0.co;2)
- New, M., Hulme, M., & Jones, P. (2000). Representing twentieth-century space–time climate variability. Part II: Development of 1901–96 monthly grids of terrestrial surface climate. *Journal of Climate*, 13(13), 2217–2238. [https://doi.org/10.1175/1520-0442\(2000\)013<2217:rtctsc>2.0.co;2](https://doi.org/10.1175/1520-0442(2000)013<2217:rtctsc>2.0.co;2)
- Norby, R. J., Warren, J. M., Iversen, C. M., Medlyn, B. E., & McMurtrie, R. E. (2010). CO<sub>2</sub> enhancement of forest productivity constrained by limited nitrogen availability. *Proceedings of the National Academy of Sciences*, 107(45), 19368–19373. <https://doi.org/10.1073/pnas.1006463107>
- Odum, E. P. (1969). The strategy of ecosystem development. *Science*, 164(3877), 262–270. <https://doi.org/10.1126/science.164.3877.262>
- Oren, R., Ellsworth, D. S., Johnsen, K. H., Phillips, N., Ewers, B. E., Maier, C., et al. (2001). Soil fertility limits carbon sequestration by forest ecosystems in a CO<sub>2</sub>-enriched atmosphere. *Nature*, 411(6836), 469–472. <https://doi.org/10.1038/35078064>
- Peñuelas, J., Poulter, B., Sardans, J., Ciais, P., van der Velde, M., Bopp, L., et al. (2013). Human-induced nitrogen–phosphorus imbalances alter natural and managed ecosystems across the globe. *Nature Communications*, 4(1), 2934. <https://doi.org/10.1038/ncomms3934>
- Rasmussen, M., Hastings, A., Smith, M. J., Agosto, F. B., Chen-Charpentier, B. M., Hoffman, F. M., et al. (2016). Transit times and mean ages for nonautonomous and autonomous compartmental systems. *Journal of Mathematical Biology*, 73(6), 1379–1398. <https://doi.org/10.1007/s00285-016-0990-8>
- Reich, P. B., Hungate, B. A., & Luo, Y. (2006). Carbon-Nitrogen Interactions in Terrestrial Ecosystems in Response to Rising Atmospheric Carbon Dioxide. *Annual Review of Ecology, Evolution, and Systematics*, 37(1), 611–636. <https://doi.org/10.1146/annurev.ecolsys.37.091305.110039>
- Running, S., Mu, Q., & Zhao, M. (2015). MOD17A2H MODIS/Terra Gross Primary Productivity 8-Day L4 Global 500m SIN Grid V006. NASA EOSDIS Land Processes DAAC. <https://doi.org/10.5067/MODIS/MOD17A2H.006>
- Sierra, C. A., Muller, M., Metzler, H., Manzoni, S., & Trumbore, S. E. (2017). The muddle of ages, turnover, transit, and residence times in the carbon cycle. *Global Change Biology*, 23(5), 1763–1773. <https://doi.org/10.1111/gcb.13556>
- Sionit, N., Mortensen, D. A., Strain, B. R., & Hellmers, H. (1981). Growth Response of Wheat to CO<sub>2</sub> Enrichment and Different Levels of Mineral Nutrition<sup>1</sup>. *Agronomy Journal*, 73(6), 1023–1027. <https://doi.org/10.2134/agronj1981.00021962007300060027x>
- Spawn, S. A., Sullivan, C. C., Lark, T. J., & Gibbs, H. K. (2020). Harmonized global maps of above and belowground biomass carbon density in the year 2010. *Scientific Data*, 7(1), 1–22. <https://doi.org/10.1038/s41597-020-0444-4>
- Taylor, J. A., & Lloyd, J. (1992). Sources and sinks of atmospheric CO<sub>2</sub>. *Australian Journal of Botany*, 40(5), 407–418. <https://doi.org/10.1071/bt9920407>
- Thornton, P. E., Lamarque, J. F., Rosenbloom, N. A., & Mahowald, N. M. (2007). Influence of carbon-nitrogen cycle coupling on land model response to CO<sub>2</sub> fertilization and climate variability. *Global Biogeochemical Cycles*, 21(4), GB4018. <https://doi.org/10.1029/2006gb002868>
- Todd-Brown, K. E. O., Randerson, J. T., Hopkins, F., Arora, V., Hajima, T., Jones, C., et al. (2014). Changes in soil organic carbon storage predicted by Earth system models during the 21st century. *Biogeosciences*, 11(8), 2341–2356. <https://doi.org/10.5194/bg-11-2341-2014>
- Todd-Brown, K. E. O., Randerson, J. T., Post, W. M., Hoffman, F. M., Tarnocai, C., Schuur, E. A. G., & Allison, S. D. (2013). Causes of variation in soil carbon simulations from CMIP5 Earth system models and comparison with observations. *Biogeosciences*, 10(3), 1717–1736. <https://doi.org/10.5194/bg-10-1717-2013>
- van Groenigen, K.-J., Six, J., Hungate, B. A., de Graaff, M. A., van Breemen, N., & van Kessel, C. (2006). Element interactions limit soil carbon storage. *Proceedings of the National Academy of Sciences*, 103(17), 6571–6574. <https://doi.org/10.1073/pnas.0509038103>
- Varney, R. M., Chadburn, S. E., Friedlingstein, P., Burke, E. J., Koven, C. D., Hugelius, G., & Cox, P. M. (2020). A spatial emergent constraint on the sensitivity of soil carbon turnover to global warming. *Nature Communications*, 11(1), 5544. <https://doi.org/10.1038/s41467-020-19208-8>
- Vitousek, P. M., Porder, S., Houlton, B. Z., & Chadwick, O. A. (2010). Terrestrial phosphorus limitation: Mechanisms, implications, and nitrogen–phosphorus interactions. *Ecological Applications*, 20(1), 5–15. <https://doi.org/10.1890/08-0127.1>
- Wang, J., Xia, J., Zhou, X., Huang, K., Zhou, J., Huang, Y., et al. (2019). Evaluating the simulated mean soil carbon transit times by Earth system models using observations. *Biogeosciences*, 16(4), 917–926. <https://doi.org/10.5194/bg-16-917-2019>
- Wang, Y., Ciais, P., Goll, D., Huang, Y., Luo, Y., Wang, Y. P., et al. (2018). GOLUM-CNP v1.0: A data-driven modeling of carbon, nitrogen and phosphorus cycles in major terrestrial biomes. *Geoscientific Model Development*, 11(9), 3903–3928. <https://doi.org/10.5194/gmd-11-3903-2018>
- Wang, Y. P., Houlton, B. Z., & Field, C. B. (2007). A model of biogeochemical cycles of carbon, nitrogen, and phosphorus including symbiotic nitrogen fixation and phosphatase production. *Global Biogeochemical Cycles*, 21(1), GB1018. <https://doi.org/10.1029/2006gb002797>
- Wang, Y. P., Kowalczyk, E., Leuning, R., Abramowitz, G., Raupach, M. R., Pak, B., et al. (2011). Diagnosing errors in a land surface model (CABLE) in the time and frequency domains. *Journal of Geophysical Research*, 116(G1), G01034. <https://doi.org/10.1029/2010jg001385>
- Wang, Y. P., Law, R. M., & Pak, B. (2010). A global model of carbon, nitrogen and phosphorus cycles for the terrestrial biosphere. *Biogeosciences*, 7(7), 2261–2282. <https://doi.org/10.5194/bg-7-2261-2010>
- Wang, Y. P., Zhang, Q., Pitman, A. J., & Dai, Y. (2015). Nitrogen and phosphorus limitation reduces the effects of land use change on land carbon uptake or emission. *Environmental Research Letters*, 10(1), 014001. <https://doi.org/10.1088/1748-9326/10/1/014001>
- Wei, N., Cui, E., Huang, K., Du, Z., Zhou, J., Xu, X., et al. (2019). Decadal Stabilization of Soil Inorganic Nitrogen as a Benchmark for Global Land Models. *Journal of Advances in Modeling Earth Systems*, 11(4), 1088–1099. <https://doi.org/10.1029/2019ms001633>
- Wieder, W. (2014). RegridDED Harmonized World Soil Database v1.2. Data set. Retrieved from <http://daac.ornl.gov>

- Wieder, W. R., Cleveland, C. C., Smith, W. K., & Todd-Brown, K. (2015). Future productivity and carbon storage limited by terrestrial nutrient availability. *Nature Geoscience*, 8(6), 441–444. <https://doi.org/10.1038/ngeo2413>
- Xia, J., Luo, Y., Wang, Y. P., & Hararuk, O. (2013). Traceable components of terrestrial carbon storage capacity in biogeochemical models. *Global Change Biology*, 19(7), 2104–2116. <https://doi.org/10.1111/gcb.12172>
- Xia, J., Luo, Y. Q., Wang, Y. P., Weng, E. S., & Hararuk, O. (2012). A semi-analytical solution to accelerate spin-up of a coupled carbon and nitrogen land model to steady state. *Geoscientific Model Development*, 5(5), 1259–1271. <https://doi.org/10.5194/gmd-5-1259-2012>
- Xia, J., & Wan, S. (2008). Global response patterns of terrestrial plant species to nitrogen addition. *New Phytologist*, 179(2), 428–439. <https://doi.org/10.1111/j.1469-8137.2008.02488.x>
- Xia, J., Yuan, W., Wang, Y. P., & Zhang, Q. (2017). Adaptive carbon allocation by plants enhances the terrestrial carbon sink. *Scientific Reports*, 7(1), 3341. <https://doi.org/10.1038/s41598-017-03574-3>
- Zaehle, S. (2013). Terrestrial nitrogen–carbon cycle interactions at the global scale. *Philosophical Transactions of the Royal Society B: Biological Sciences*, 368(1621), 20130125. <https://doi.org/10.1098/rstb.2013.0125>
- Zaehle, S., & Dalmonech, D. (2011). Carbon–nitrogen interactions on land at global scales: Current understanding in modelling climate biosphere feedbacks. *Current Opinion in Environmental Sustainability*, 3(5), 311–320. <https://doi.org/10.1016/j.cosust.2011.08.008>
- Zaehle, S., & Friend, A. D. (2010). Carbon and nitrogen cycle dynamics in the O-CN land surface model: 1. Model description, site-scale evaluation, and sensitivity to parameter estimates. *Global Biogeochemical Cycles*, 24(1), GB1005. <https://doi.org/10.1029/2009GB003521>
- Zhang, Q., Wang, Y. P., Pitman, A. J., & Dai, Y. J. (2011). Limitations of nitrogen and phosphorus on the terrestrial carbon uptake in the 20th century. *Geophysical Research Letters*, 38(22), L22701. <https://doi.org/10.1029/2011GL049244>
- Zhang, Y., Xiao, X., Wu, X., Zhou, S., Zhang, G., Qin, Y., & Dong, J. (2017). A global moderate resolution dataset of gross primary production of vegetation for 2000–2016. *Scientific Data*, 4(1), 170165. <https://doi.org/10.1038/sdata.2017.165>
- Zhu, Q., Riley, W. J., Tang, J., Collier, N., Hoffman, F. M., Yang, X., & Bisht, G. (2019). Representing nitrogen, phosphorus, and carbon interactions in the E3SM land model: Development and global benchmarking. *Journal of Advances in Modeling Earth Systems*, 11(7), 2238–2258. <https://doi.org/10.1029/2018ms001571>